Journal of Visualization, Vol. 10, No. 4 (2007)389-396

Regular Paper

Oscillatory Thermal Structures in a Reattaching Jet Flow

Narayanan, V.*

* School of Mechanical, Industrial and Manufacturing Engineering, Oregon State University, 204 Rogers Hall, Corvallis, Oregon 97331-6001, USA. E-mail: vinod.narayanan@oregonstate.edu

Received 21 March 2007
Revised 15 August 2007

Abstract : Spatially varying surface temperature oscillations in a nominally steady reattaching slot jet at a Reynolds number (Re) of 5000 are analyzed using Proper Orthogonal Decomposition (POD) for two nozzle–to–surface spacings, and three exit openings of the nozzle. The surface temperature data in these experiments were recorded using infrared thermography at a frequency of 20 Hz along two selected lines on the impingement surface corresponding to geometrically similar and dissimilar regions within the reattachment curtain. The magnitude of temperature oscillations were found to increase with an increase in exit opening for the larger nozzle spacing. The POD analysis results indicate that a majority of the temperature flucutations are well captured by 15 dominant modes. In many cases, the three dominant modes accounted for approximately 60 percent of the variance in surface temperature fluctuation.

Keywords : Infrared (IR) Thermography, thermal structures, reattachment, jet, temperature fluctuations, Proper Orthogonal Decomposition (POD).

1. Introduction

Because of its importance in cooling, heating, and drying applications, jet impingement heat transfer has been studied extensively over the past five decades. Both experimental and numerical studies on jet impingement have been well documented in literature (Martin, 1977; Viskanta, 1993). Modifications to conventional circular or slot jets have been proposed by several researchers as a means to enhance impingement heat transfer. Some of these modifications include placing devices within the nozzle to cause swirl (Huang et al., 1998), periodic forcing (Hill and Greene, 1977; Hasan and Hussain, 1982; Tesar and Travnicek, 2006), and causing the jet to reattach (Page et al., 1988). To document enhancements in heat transfer obtained by these new geometries there is a need to quantify not only the time and/or spatially averaged data, but also flow structure and surface temperature on a spatially and temporally resolved scale. Time–averaged, but spatially local measurements, by providing the spatial gradients in temperature, help to elucidate the mean flow structure and local heat transfer, thereby allowing for design of the geometry of the jets, the nozzle–to–surface spacing, and the number of jets required for a particular heating, cooling, or drying application. Spatially local and time varying temperature measurements can, in addition, help to determine the local fluctuations in the nominally mean jet flow that could be expected in the use of a particular nozzle and configuration. Sometimes, these spatial data are rather complex and/or noisy, and methods are needed to elucidate its structure.

The purpose of this paper is to report and analyze temporal oscillations in wall temperature for a nominally steady reattachment jet. The focus of this study is on the recirculation region, the region of low heat transfer, with the aim of determining the flow and thermal structures, and with such

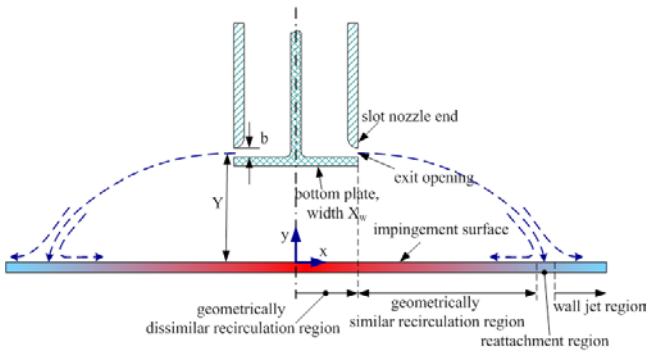

Fig. 1. Schematic of the reattachment jet.

understanding, identifying methods to enhance heat transfer rate in this region. Figure 1 shows a schematic of the cross section of the reattachment nozzle and the jet that emanates from it. The gap that is formed between the bottom plate and the slot nozzle end, through which the jet emanates is referred to as the exit opening. The aspect ratio of the slot is 20:1, with circular ends to facilitate formation of a closed reattachment curtain. The jet exits parallel to, and reattaches on, the surface along the major and minor axes. Thus, the recirculating flows on both sides of the major axis (x = 0.0) interact with each other beneath the bottom plate of the nozzle. The flow region beneath the bottom plate represents a geometrically dissimilar region, see Narayanan et al. (2004). Because the jet flow was unconfined at the radial ends, an annular reattachment region was formed, which was rectangular in most of the region along the major axis, and turned radial towards the ends. The circular ends, which help to maintain the sub-atmospheric recirculation region, are an important aspect of this unconfined jet geometry. An unconfined jet was studied here since it is the most practical geometry for use in a process application, where the nozzle needs to be located away from the impingement surface.

A Proper Orthogonal Decomposition (POD) method is used to analyze and compare the trends in the impingement surface temperature fluctuations. Data for a very close spacing of $Y/X_w = 0.25$ and a farther spacing of $Y/X_w = 1.0$ are analyzed, where X_w is the width of the bottom plate of the reattachment nozzle. The former spacing corresponds to a large gradient in spatial temperature distribution along the x coordinate, while the latter corresponds to an unstable reattachment. Near–wall flow structure and/or the impingement surface temperature have been documented in several studies for jet impingement (VanFossen and Simoneau, 1987; Yokobori et al., 1988; Kataoka et al., 1994). Sakakibara et al. (1997) measured, simultaneously, the near–wall vortex structure and fluid temperature distribution in the impingement region. They observed that counter–rotating vortex pairs swept cold fluid toward the wall, and ejected high–temperature fluid toward the outer region. The wall temperature in the ejection region, located beneath the vortex pair was higher than in the region between the vortex pairs, where the cold fluid directly impinged on the surface. They indicated that enhanced heat transfer in the impingement region was likely due to the amplification of vorticity due to its stretching by the accelerating mean flow in the streamwise direction.

Narayanan et al. (2004) studied the mean flow field and heat transfer characteristics of a reattaching slot jet of aspect ratio 20:1 at a close nozzle–to–surface spacing of $Y/X_w = 0.25$ and a farther spacing of $Y/X_w = 0.75$. Spatial distributions of local temperature, recorded at 1 frame per second, were subtracted from one another to create differential temperature maps of the surface. These maps revealed that the location of the hot and cold spots were different for the two nozzle spacings considered. Whereas hot and cold spots for the $Y/X_w = 0.25$ were restricted to an annular region surrounding the bottom plate, for the larger spacing, the spots were observed throughout the recirculation region.

2. Nomenclature

a^k expansion coefficient or principle component amplitude
b nozzle exit opening (m)
D_h hydraulic diameter of the nozzle; $D_h = 2b$ (m)
F matrix of time series fluctuating temperature data (^oC)

f_k fraction of covariance determined by mode k
R covariance matrix
Re Reynolds number, based on D_h
T temperature (^oC)
X_w width of the nozzle bottom plate (m)
x streamwise coordinate along the minor axis of the nozzle; x = 0.0 corresponds to the nozzle major axis on the impingement surface (m)
Y nozzle–to–surface spacing along the y axis, measured from the jet exit centerline (m)
z spanwise coordinate along the major axis of the nozzle, z = 0.0 location corresponds to the nozzle minor axis on the impingement surface (m)

Greek

λ spacing between thermal streaks (m) or eigenvalue
ψ^k eigenfunction

Subscripts

f fluctuating component
i time index (0 to 1655)
j z-direction spatial index
m mean

3. Experimental Facility and Procedure

A detailed description of the experimental set–up and test section are provided in Narayanan et al. (2004). Briefly, dried and filtered compressed air was supplied to a plenum through two settling tanks and pressure regulators. The mass flow rate was measured with a sonic nozzle at the exit of the last settling tank. The plenum had a series of screens and a honeycomb, followed by a convergent section. The flow exited the plenum through an end plate with a contoured slot of aspect ratio 20:1. A schematic of the heat transfer test section is shown in Fig. 2. The impingement surface consisted of a constant heat flux surface surrounded by Plexiglas end plates on all sides. The test section was 63.5 cm long and 63.5 cm wide, and consisted of a central heated test section made of a 25 μm thick inconel 600 foil 38.1 cm long and 38.1 cm wide, stretched tightly between two solid copper bus bars. The foil was electrically heated by a DC power supply and represents a near–constant heat flux surface. The width of the nozzle slot and bottom plate were 12.7 mm and 25.4 mm, respectively.

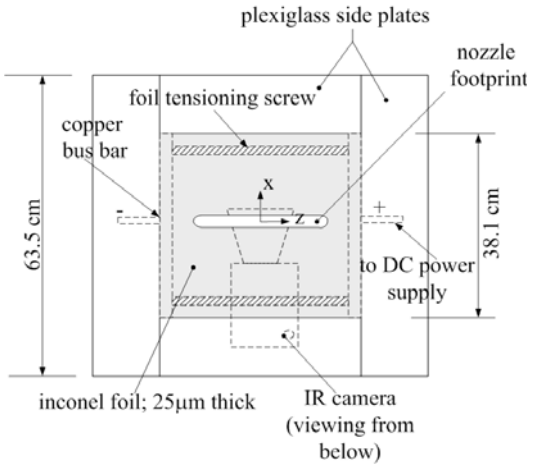

Fig. 2. Schematic of heat transfer test section.

Local surface temperatures were measured non–intrusively with a 8–13 μm wavelength infrared (IR) camera (Mikron Inc., model 6T62 thermotracer) from beneath the foil; see Fig. 2. The foil bottom was painted with flat black paint for high surface emissivity. For visualizing temperature fluctuations, the imager was operated in a time trace mode in which the imaging optics scanned across a single horizontal line encompassing 256 spatial locations over 206 equal time intervals for each frame recorded. In this mode, temperatures could be recorded at a frame rate (or an equivalent line scan rate) ranging from 1/60 frames per second (3.45 Hz) to 1 frame per second (207 Hz). Because the time response of the combined inconel foil and black paint layer was estimated to be about 20 Hz, only data recorded with a line scan rate of 20 Hz is analyzed here. Along the chosen x = constant line, eight frames of data were collected and stored in the imager memory before being transferred to the computer through a GPIB interface. A total of 8 frames provided 1656 temperature values at discrete time intervals at each of the 256 locations along a horizontal line.

4. Data Analysis

A POD analysis was performed on discrete temperature data obtained from IR images. For the analysis, only the central 106 locations along the z–axis are chosen because they represent the planar region of the jet. Recall that the ends of the nozzle were circular and the jet was unconfined at its ends. The analysis technique outlined by Bjornsson and Venegas (1997) was applied in Matlab®. The oscillatory (also referred to in this paper as "fluctuating") component of temperature at each location was found using

$$T_{f,ij} = T_{ij} - T_{m,j} \tag{1}$$

The time series oscillatory temperature data at each location was arranged as a column vector in a matrix F. The covariance matrix, R, of F was calculated as

$$R = F^t \times F \tag{2}$$

Solving the eigenvalue problem for this matrix gives POD eigenfunctions, ψ^k , and its associated eigenvalue, λ_k . The eigenfuctions are arranged in decreasing order of their eigenvalues. The fraction of the total variance in R as explained by a particular mode can be determined by dividing its eigenvalue by sum of all the eigenvalues,

$$f_k = \lambda_k \Big/ \sum_{j=1}^{M} \lambda_j \tag{3}$$

Hence, the first modes represent the largest or the most dominant fluctuating thermal features in the temperature field. The expansion coefficients or the amplitudes, a^k of the kth mode can be found by projecting F onto the kth eigenfunction,

$$a^k = F \times \psi^k \tag{4}$$

The expansion coefficients provide the variation of that POD mode with time. The original data can be constructed from the modes using

$$F = \sum_{j=1}^{n} a^k \psi^k \tag{5}$$

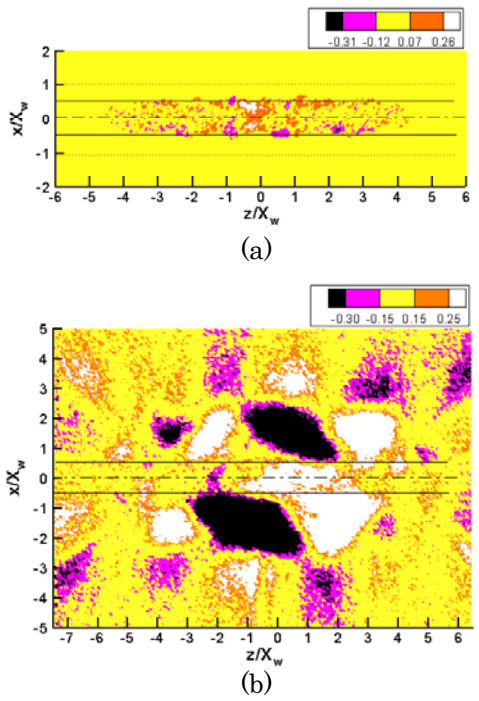

Fig. 3. Differential temperature maps at Re = 10,000 for nozzle spacing of (a) Y/X_w = 0.25 and (b) Y/X_w = 1.00.

5. Results and Discussion

Results of surface temperature fluctuations caused by the reattaching jet flow for a nozzle exit Reynolds number (Re) of 5,000 at two nozzle–to–surface spacings, Y/X_w = 0.25 and 1.00 are first presented. The exit opening is fixed at b/X_w = 0.10. Experiments were also performed at two higher Re of 10,000 and 15,000. In general, the trends remained the same at these higher Re; however, the percent variance in the fluctuating temperature data that is explained by the first 15 dominant modes decreased with an increase in Re. Variations in fluctuating temperatures due to changes to the exit opening of b/X_w = 0.10 by ± 50 percent are presented next at a fixed nozzle spacing of Y/X_w = 1.00.

Data of temperature–time traces are typically presented at specific x/X_w locations along the impingement surface, within the reattachment region. These locations correspond to regions of interest identified by the differential temperature maps recorded at Re = 10,000, which are shown in Figs. 3(a) and (b). The differential temperature maps were formulated from a series of spatial images recorded at 1 frame per second by subtracting the image recorded at time *(t)* seconds from the image at time *(t-1)* seconds.

Table 1. Summary of the percent variances contained in dominant modes.

Re	Y/X_w	b/X_w	x/X_w	Fig.	Mode1	Mode 2	Mode 3	Mode 4	Modes 1-15
5,000	0.25	0.10	0.00	4	52.0	10.8	4.2	3.2	78.7
5,000	0.25	0.10	-0.65	5	37.2	13.7	6.5	4.2	85.2
5,000	1.00	0.10	0.00	6	43.3	18.0	6.8	4.8	86.1
5,000	1.00	0.10	-0.71	7	34.9	24.2	11.0	3.8	84.8
5,000	1.00	0.05	0.00	8	34.6	19.8	8.3	5.7	85.3
5,000	1.00	0.15	0.00	9	59.2	24.7	4.6	2.1	96.4

Because the IR camera was a line scanner, the observed structures could be spatially and temporally distorted. Nevertheless, these images clearly indicate the presence of large–scale thermal structures within the recirculation region at both spacings. At the lower nozzle spacing, hot and cold temperature spots, typically of the size between $0.4X_w$ and $0.6X_w$, are arranged in an annular ring around the bottom plate. The intensity and size of these structures increases significantly with nozzle–to–surface spacing. Also, for the $Y/X_w = 1.00$ spacing, hot and cold streaks are observed past reattachment region ($x/X_w > 2.7$), indicating the possibility of periodic flapping of the reattachment curtain that causes exhaust of warm air at certain spanwise locations and entrainment of the cooler ambient air at other locations. Note that at this nozzle spacing, flow visualization revealed an unstable reattachment curtain. Based on these images, time series data were recorded and analyzed at streamwise lines corresponding to the projected nozzle centerline on the surface, $x/X_w = 0$ and the locations of large differential temperatures for both spacings.

Figures 4(a) and 5(a) present temperature fluctuation maps for the low nozzle spacing at the centerline, $x/X_w = 0.00$, and at $x/X_w = -0.65$, respectively. The exit Re was fixed at 5,000 and the exit opening was $b/X_w = 0.10$. Temperature fluctuations were determined from time traces by using Eq. (1). Note that the contour plots in all figures have the same scale to permit a direct comparison of the magnitudes of temperature fluctuations. The time traces are consistent with trends of spatial thermal structures shown in Fig. 3(a); fewer structures are discerned at the centerline as opposed to the downstream location. Figs. 4(b)–(e) and 5(b)–(e) show the reconstruction of data using the first four modes of POD at the two locations. At both locations, the first mode mainly captures the temporal but not the spatial variations in temperature; this observation is more pronounced at the $x/X_w = -0.65$ location. A comparison of the time spacing between the occurrence of the thermal

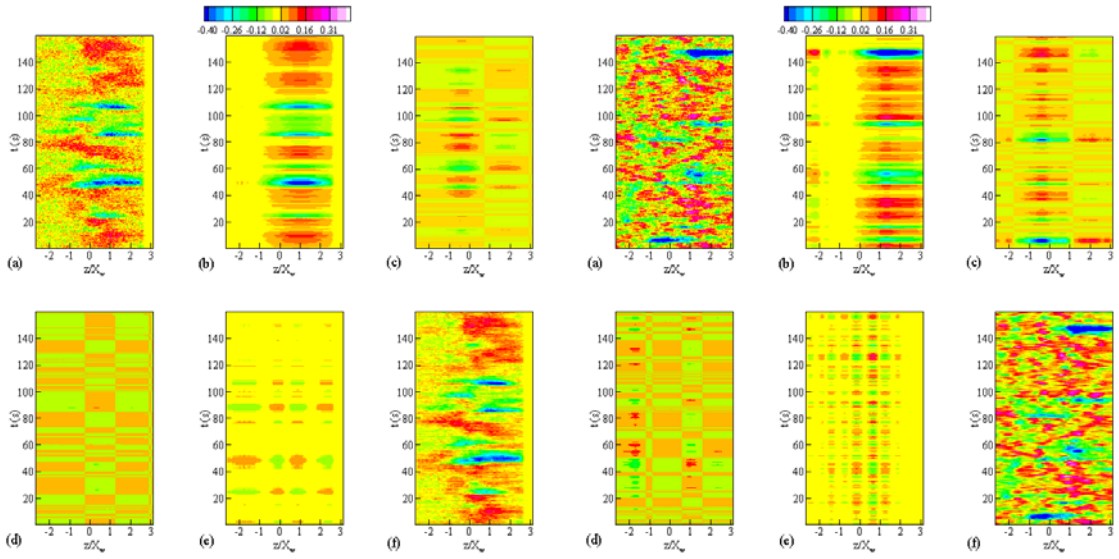

Fig. 4. Time traces of fluctuating temperature distribution at the centerline ($x/X_w = 0.00$) for $Y/X_w = 0.25$, $b/X_w = 0.10$, at a Re = 5,000. (a) original data; reconstructions using (b) mode 1; (c) mode 2; (d) mode 3; (e) mode 4; and (f) 15 most energetic modes.

Fig. 5. Time traces of fluctuating temperature distribution at $x/X_w = -0.65$ for $Y/X_w = 0.25$, $b/X_w = 0.10$, at a Re = 5,000. (a) original data; reconstructions using (b) mode 1; (c) mode 2; (d) mode 3; (e) mode 4; and (f) 15 most energetic modes.

fluctuations at the centerline and downsteam location for the first mode exhibits a higher frequency of events at the downstream location. Table 1 summarizes the percent of variance captured by modes 1, 2, 3, and 4, and the cumulative modes 1 to 15. This table indicates that the first mode captures a larger percent of the variance at the center than at x/X_w = -0.65. For the x/X_w = -0.65 location, the fourth mode reconstruction clearly indicates the spatial variations consistent with that shown in Fig. 3(a), with alternating hot and cold streaks of about 0.5 X_w width. The width of these structures are similar to those produced by near–wall counter-rotating vortices in the impingement region of a slot jet (Sakakibara et al., 1997). Mean flow field data were recorded using laser Doppler anemometry only at z/Z_w = 0.0 and hence do not reveal such vortex pairs (Narayanan et al., 2004). Also, an instantaneous whole–field imaging technique is necessary to reveal such transient near–wall structures that cause the associated temperature fluctuations.

Figures 4(f) and 5(f) present data reconstruction using the 15 most dominant modes from the POD analysis, and a comparison of the data and these reconstructions indicate that in excess of 75 percent of the dominant temperature fluctuations are captured using these modes, with the first four modes accounting for over 60 percent of the variance in the dataset. The fluctuations that are not captured are predominantly high–frequency events that can be attributed to the noise in the temperature measurement using the IR camera. In this regard, POD reconstructions from the dominant modes can be applied as a filter to a noisy dataset.

Figures 6(a) and 7(a) present the temperature oscillations for Y/X_w = 1.0 nozzle spacing at the centerline (x/X_w = 0.00) and at x/X_w = -0.71, respectively. The latter location, as seen from the discussion related to Fig. 3(b), is within the recirculation region. The location of the large–scale thermal structures seen in Fig. 3(b) and 6(a) at x/X_w = 0.00 are consistent. Whereas the first mode at x/X_w = 0.00 identifies two major spatial structures at this location; at x/X_w = 0.71, this mode captures only variations of the spatial structure between $-2 < z/Z_w < 0$. At this location, the second mode captures variations in the thermal structure location between z/Z_w of 1 and 3. Figures 6(f) and 7(f), which present reconstructions of the 15 most dominant modes indicate that the reconstructed data represent the major spatial and temporal variations of original data; Table 1 indicates that approximately 85 percent of the variance is explained by a combination of these modes.

To quantify the effect of variation of exit opening on temperature oscillations, results of the POD analysis at two locations for the slot jet reattachment flow at a Re of 5,000 and the largest nozzle spacing of Y/X_w = 1.00 for three exit openings of b/X_w = 0.05, 0.10, and 0.15 are presented.

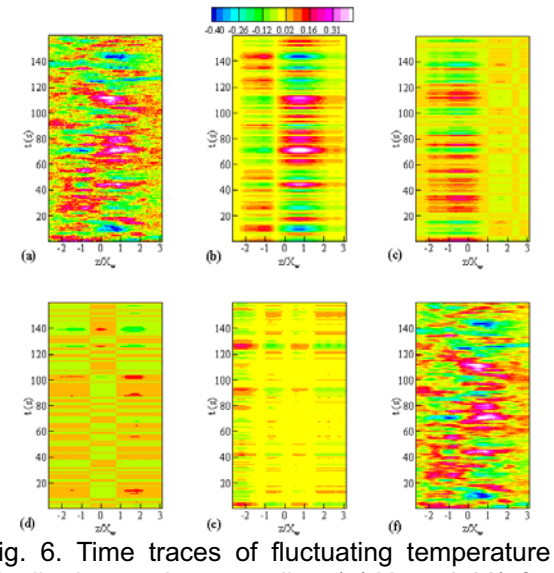

Fig. 6. Time traces of fluctuating temperature distribution at the centerline (x/X_w = 0.00) for Y/X_w = 1.00, b/X_w = 0.10, at a Re = 5,000. (a) original data; reconstructions using (b) mode 1; (c) mode 2; (d) mode 3; (e) mode 4; and (f) 15 most energetic modes.

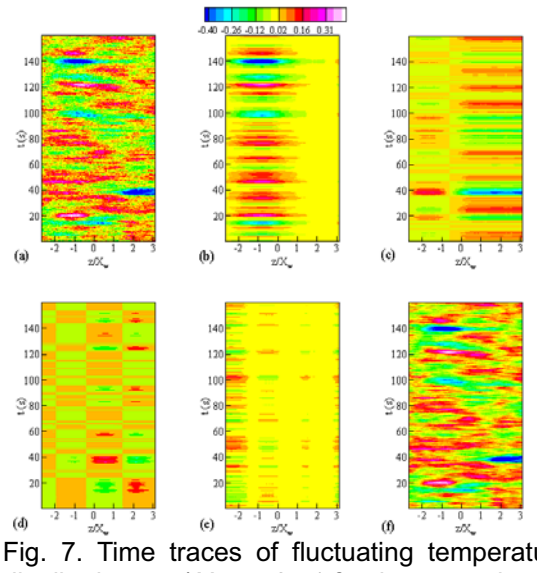

Fig. 7. Time traces of fluctuating temperature distribution at x/X_w = - 0.71 for the reattachment jet at a spacing, Y/X_w = 1.00, b/X_w = 0.10, at a Re = 5,000. (a) original data; reconstructions using (b)mode 1; (c) mode 2; (d) mode 3; (e) mode 4; and (f) 15 most energetic modes.

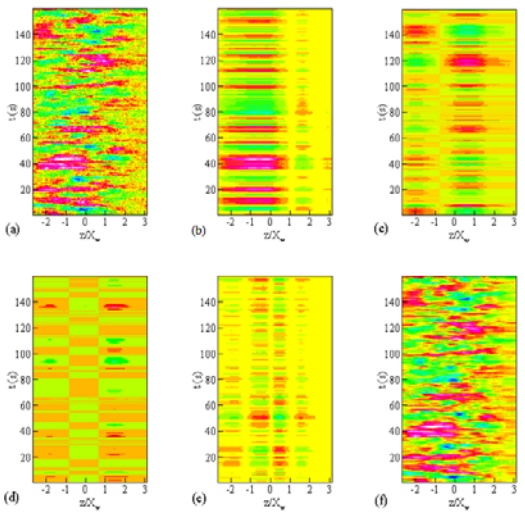

Fig. 8. Time traces of fluctuating temperature distribution at the centerline (x/ X_w = 0.00) for Y/ X_w = 1.00, b/ X_w = 0.05, at a Re = 5,000. (a) original data; reconstructions using (b) mode 1; (c) mode 2; (d) mode 3; (e) mode 4; and (f) 15 most energetic modes.

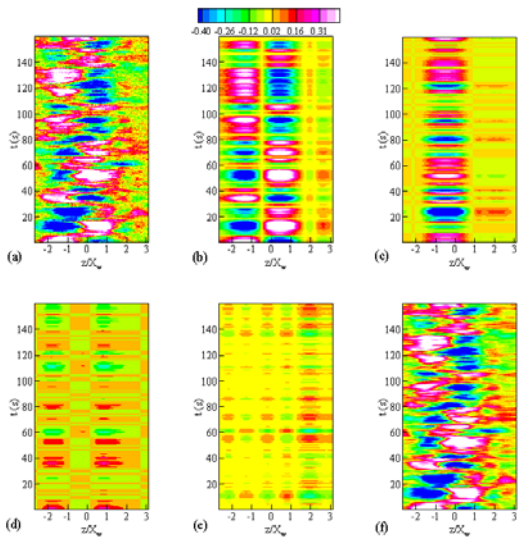

Fig. 9. Time traces of fluctuating temperature distribution at the centerline (x/ X_w = 0.00) for Y/ X_w = 1.00, b/ X_w = 0.15, at a Re = 5,000. (a) original data; reconstructions using (b) mode 1; (c) mode 2; (d) mode 3; (e) mode 4; and (f) 15 most energetic modes.

Figures 8 (a) and 9(a) show the temperature fluctuations for the exit openings of b/X_w = 0.05 and 0.15, respectively; these exit openings are perturbations to the nozzle configuration whose temperature fluctuations are shown in Fig. 6(a). These variations are denoted at the major axis, x/X_w = 0.00. Little variation can be discerned between the temperature fluctuation patterns for the b/X_w = 0.05 and 0.10 exit openings. In contrast, at the largest exit opening (Fig. 9(a)), the intensity of fluctuations increases with a noticeable decrease in frequency of the thermal spots. The temperature data, as well as the first mode, clearly indicate the presence of two large cold and hot thermal spots at any given time that are of the width of about 1X_w to 1.5X_w. However, the increase in magnitude of thermal spots could be indicative of a more unstable reattachment for the larger exit opening nozzle due to a decreased exit velocity of the jet for identical Re as the lower openings. It should be mentioned that because the temperature data were recorded at 20 Hz, any conclusion with regard to the frequency of thermal events from the time traces can be misleading due to a potential for aliasing of data. Figures 6(b)–(e), 8(b)–(e), and 9(b)–(e) represent reconstructions of fluctuations using modes 1 to 4, respectively for the three exit openings of b/X_w = 0.10, 0.05, and 0.15 respectively. The contribution of mode 1 to the total variance (see Table 1) increases with an increase in exit opening. Also, the variance obtained from the dominant 15 modes is very large for the largest exit opening (96.4 percent) compared to the other two spacings (about 86 percent).

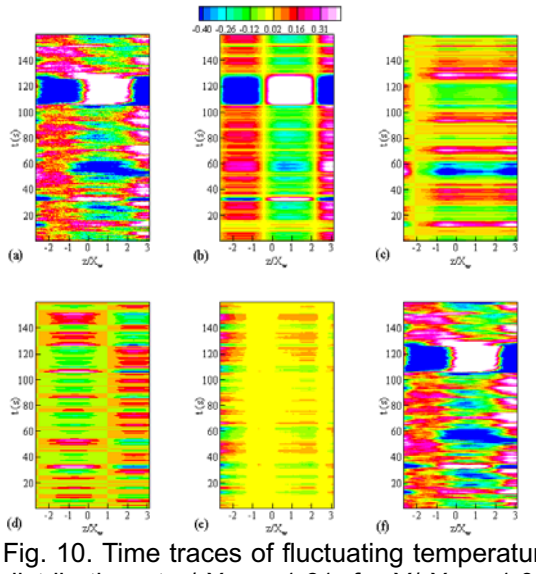

Fig. 10. Time traces of fluctuating temperature distribution at x/ X_w = -1.61, for Y/ X_w = 1.00, b/ X_w = 0.15, and Re of 5,000. (a) original data; reconstructions using (b)mode 1; (c) mode 2; (d) mode 3; (e) mode 4; and (f) 15 most energetic modes.

Figure 10(a) shows the temperature fluctuations at a further downstream distance of x/X_w = -1.61 from the nozzle centerline for the Y/X_w = 1.00 and b/X_w = 0.15 reattachment jet. Note that this location is still within the recirculation region. The spatial two–dimensional temperature difference

map shown in Fig. 3(b) indicates that this location corresponds closely to the center of the large hot and cold thermal spots; spanning approximately 2.5 X_w. The time trace shown in Fig. 10(a) corroborates well with the width of the thermal spots observed from the differential map; Fig 3(b). Figures 10(b)–(e) show the reconstructions of data using the first four modes, respectively, which indicate that the first mode captures most of the large spatial and temporal variance variations. Table 1 indicates that the first mode account for almost 70 percent, and the 15 dominant modes for almost 98 percent, of the variance at this location.

6. Conclusions

A Proper Orthogonal Decomposition (POD) analysis was performed on the scalar temperature fluctuation dataset obtained using infrared thermography. Two–dimensional differential temperature maps were used to identify locations of interest for time trace measurements. In general, thermal spots identified by the differential temperature maps showed good correspondence with the time traces recorded at specific streamwise locations within the recirculation region. Results from the time–trace POD analysis indicate that the 15 most dominant modes account for larger than 75 percent of the variance in the datasets. The temperature variations for the large nozzle–to–surface spacing of $Y/X_w = 1.00$ and large exit opening of $b/X_w = 0.15$ were the largest (in magnitude); the two most dominant modes efficiently captured about 82 percent of the variations in the data at the centerline and two downstream locations.

Acknowledgements

The author would like to thank Vishal Patil for help in developing the data analysis program.

References

Bjornsson, H. and Venegas, S. A., A Manual for EOF and SVD Analyses of Climatic Data, CCGCR Report, 97-1 (1997).

Hasan, M. A. Z. and Hussain, A. K. M. F., The Self-excited Axisymmetric Jet, Journal of Fluid Mechanics, 115 (1984), 59-89.

Hill, W. G. and Greene, P. R., Increasing Turbulence Jet Mixing Rates Obtained by Self-Excited Acoustic Oscillations, Trans. of ASME Journal of Fluids Engineering, 99 (1977), 520-525.

Huang, L. and El-Genk, M. S., Heat Transfer and Flow Visualization Experiments of Swirling, mulit-channel, and Conventional Impinging Jets, International Journal of Heat and Mass Transfer, 41-3 (1998), 583-600.

Kataoka, K., Kawasaki, H., Tsujimoto, M. and Ohmura, N., Effect of Longitudinal Vortices on Heat Transfer a Two-Dimensional Jet Strikes Against, Proceedings of the Tenth International Heat Transfer Conference (Brighton, U.K.), 3-4EC-8 (1994), 31-36.

Martin, H., Heat and Mass Transfer between Impinging Gas Jets and Solid Surfaces, Advances in Heat Transfer, 13 (1977), 1-60.

Narayanan, V., Seyed-Yagoobi, J. and Page, R. H., Surface Flow Structure, Turbulence, and Heat Transfer in a Reattaching Slot Jet Flow, International Journal of Heat and Mass Transfer, 47-24 (2004), 5219-5234.

Page, R. H., Hadden, L. L. and Ostowari, C., A theory of Radial Jet Reattachment Flow, AIAA Journal of Thermophysics and Heat Transfer, 27-11 (1988), 1500-1505.

Sakakibara, J., Hishida, K. and Maeda, M., Vortex Structure and Heat Transfer in the Stagnation Region of an Impinging Plane Jet (Simultaneous Measurements of Velocity and Temperature Fields by Digital Particle Image Velocimetry and Laser-Induced Fluorescence), International Journal of Heat and Mass Transfer, 40-13 (1997), 3163-3176.

Tesar, V. and Travnicek, Z., Increasing Heat and/or Mass Transfer Rates in Impinging Jets, Journal of Visualization, 8-2 (2005), 91-98.

VanFossen, G. J. and Simoneau, R. J., A Study of the Relationship Between Free-Stream Turbulence and Stagnation Region Heat Transfer, Journal of Heat Transfer, 109 (1987), 10-15.

Viskanta, R., Heat Transfer to Impinging Isothermal Gas and Flame Jets, Experimental Thermal and Fluid Science, 6 (1993), 111-134.

Yokobori. S., Kasagi, N., Hirata, M. and Nishiwaki, N., Role of Large-Scale Eddy Structure on Enhancement of Heat Transfer in Stagnation Region of Two-Dimensional, Submerged, Impinging Jet, Sixth International Heat Transfer Conference (Toronto, Canada), 5 (1978), 305-310.

Author Profile

Vinod Narayanan: He received his Ph.D. in Mechanical Engineering from Texas A&M University in 2001. Since 2001, he has been an Assistant Professor at Oregon State University, Corvallis, USA. He has worked for over 10 years in the field of jet impingement flow and heat transfer for thermal management and drying applications, and in non-intrusive thermal and flow imaging and measurements. His current research interests include experimental studies of microscale single and two-phase flows, and the use of passive means to enhance fluid and thermal transport.